Energy Storage Materials 49 (2022) 135–143

Contents lists available at ScienceDirect

Energy Storage Materials

journal homepage: www.elsevier.com/locate/ensm

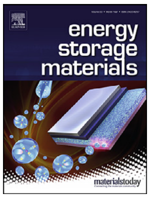

Li plating on alloy with superior electro-mechanical stability for high energy density anode-free batteries

Xiancheng Wang[a], Yufang He[b], Shuibin Tu[a], Lin Fu[a], Zihe Chen[a], Shiyu Liu[a], Zhao Cai[a], Li Wang[b], Xiangming He[b], Yongming Sun[a,*]

[a] *Wuhan National Laboratory for Optoelectronics, Huazhong University of Science and Technology, Wuhan 430074, China*
[b] *Institute of Nuclear and New Energy Technology, Tsinghua University, Beijing 100084, China*

ARTICLE INFO

Keywords:
Anode-free
Electro-mechanical stability
Current collector
Lithium-metal alloy interface

ABSTRACT

Anode-free batteries possess high energy density and avoid the use of reactive Li during battery fabrication, and thus are highly desirable for high energy density batteries. However, they encounter fast failure due to the inferior electrochemical reversibility. One main reason is the fast inactive Li accumulation caused by the coupling of side reactions and mechanics during complicated Li plating/stripping processes, among which, mechanical stability of plated Li on current collector is crucial but often ignored. To achieve good electro-mechanical stability, we construct a stable lithium-metal alloy interphase for Li plating, which sharps the Li deposition morphology and enhances the connection with deposited Li. The Li-metal alloy possesses reduced Li nucleation energy barrier and strong bonding with metallic Li, which enables dense and chunky Li deposits with firm connection with the substrate in sharp contrast the fully peeling off of metallic Li for bare Cu after 50 Li plating/stripping cycles. A Li-Sn alloy-modified Cu anode displays stable Li plating/stripping cycling with average Coulombic efficiency of 94.1% for 400 cycles at 1 mA cm^{-2} and 1 mAh cm^{-2}, significantly outperforming the bare Cu electrode. As a demonstration, in an anode-free cell with Li rich Mn-based cathode, 16.7% increase in capacity and 14.1% increase in capacity retention for 20 cycles are achieved using alloy-modified anode. This sheds new insights on the improvement of dynamic mechanical stability between Li deposits and current collector by regulating Li plating and its connection with the current collector and guides the design of high-performance initial-Li-free anode.

1. Introduction

Lithium (Li) metal batteries are considered as one of the most promising rechargeable Li-based batteries with high energy density, due to the highest specific capacity (3860 mAh g^{-1}) and lowest working potential (−3.04 V vs. standard hydrogen electrode) of metallic Li anode [1–4]. To fully explore the advantage of high energy density, it is highly desirable to integrate ultrathin Li metal anode (e.g., < 25 μm) or even initial-Li-free anode [5–7]. However, ultrathin Li metal suffers poor mechanical processability, high chemical reactivity with moisture and oxygen in ambient condition, and poor electrochemical reversibility. In this respect, anode-free batteries with initial-Li-free anode could avoid the direct use of metallic Li and maximize the battery energy density, where the cathodes provide active Li, and metallic Li is deposited on current collectors during the battery charge process and dissolved during the subsequent battery discharge process [8,9]. Note that the electrochemical Li plating behavior on current collectors plays crucial role in the electrochemical reversibility of the initial-Li-free anode [10,11]. Dendritic and porous Li deposits with inferior mechanical durability and electrochemical reversibility tend to form during Li plating. Dendritic metallic Li with high surface area reacts with electrolyte, which generates abundant solid electrolyte interphase (SEI) on its surface. During Li stripping, Li dissolution can take place from the "root" of Li dendrite, and inactive metallic Li residual wrapped by SEI may be produced due to the mechanical/physical connection failure and loss of electronic contact with the current collector [1,12]. The active Li and electrolyte would be quickly consumed, and the inactive metallic Li would aggravate the lithium-ion diffusion barrier, which deteriorate the Coulombic efficiency and eventually lead to fast failure of anode-free batteries [13,14]. Thus, it is urgent to suppress the formation of inactive metallic Li, and improve mechanical stability and electrochemical reversibility of initial-Li-free anode.

The ideal electrochemical Li plating/stripping behavior for initial-Li-free anode involves the formation of uniform and dense electrochemical Li deposition layer with good mechanical connection with the current collector, and its complete dissolution. There exists large discrepancy

---

[*] Corresponding author.
E-mail address: yongmingsun@hust.edu.cn (Y. Sun).

https://doi.org/10.1016/j.ensm.2022.04.009
Received 12 December 2021; Received in revised form 28 February 2022; Accepted 4 April 2022

for metallic Li plating on different substrates [15,16]. Taking Li metal and Cu substrates as model systems that are mostly investigated, they both show large lithium nucleation overpotential, dendritic growth of metallic Li, and low Coulombic efficiency in widely used carbonate electrolyte [17,18]. Electrolyte additives and Cu substrate interphase design can regulate the Li plating/stripping behavior and improve the electrochemical reversibility [4,19,20]. Typically, gold (Au) and silver (Ag) species deliver low Li nucleation overpotential. Through structure designs with Au and Ag on substrates, electrochemical Li plating behaviors are significantly improved, including carbon hollow particles with implanted Au nanoparticles, and Ag@polydopamine nanoparticles protected by graphene oxide [21,22]. However, Au and Ag possess high cost, and they would dissolve into Li during Li plating and precipitate out during Li dissolution, leading to possible structural instability of the electrodes during long-term cycling [16]. Thus, it is highly desirable to explore advanced current collectors that could regulate Li metal plating with high electro-mechanical stability and low cost. Besides, the introduction of lithiophilic phases (e.g., lithiated carbon materials and alloys) in Li has been improved an effective approach to stabilize Li plating behavior [23,24].

It still remains unclear that whether and how the substrate can regulate the electro-mechanical stability of metallic Li, and improve the electrochemical performance. Li could form stable alloys with various metal materials that have no (or ultra-low) solubility in metallic Li, such as tin (Sn), antimony (Sb), and zinc (Zn) [21], and thus would not have the dissolution problems that novel metals (e.g., Au and Ag) face. Using current collectors with such metal species, lithiophilic Li-metal (Li-M) alloys would be first in situ formed before Li plating [25,26]. Thus, in-plane growth of metallic Li on such Li-M alloy modified substrates can be expected, and thus good electro-mechanical stability could be realized. We emphasize that current collector with plane geometry is ideal for Li metal plating in comparison to other forms, such as three-dimension (3D) porous structures, since it is beneficial for producing dense Li metal deposition layer with small accessible surface area to liquid electrolyte, high packing density and good mechanical stability [27,28]. Here, we showed the successful design of using Li-Sn alloy interphase on commercial Cu foil in improving the electro-mechanical stability of initial-Li-free anode. The low Li nucleation energy barrier on Li-Sn alloy and high binding energy between Li and Li-Sn alloy ensured the dense and in-planar metallic Li plating with good electro-mechanical stability. The Li-Sn alloy modified Cu electrode exhibited high electrochemical reversibility for 400 cycles at 1 mA cm^{-2} and 1 mAh cm^{-2} with average CE of 94.1% in a regular carbonate electrolyte, and the deposited Li metal layer remained intact and was closely contacted with the Cu foil on cycling. In contrast, the bare Cu electrode displayed much lower average CE of 82.4%, and failed within 70 cycles, where the Li deposits peeled easily after 50 cycles. In an anode-free batteries with Li rich Mn-based cathode, we showed 16.7% increase in cycling capacity and 14.1% increase in capacity retention for 20 cycles by replacing bare Cu anode with Li-Sn alloy modified Cu foil anode, suggesting the success of the design of electro-mechanically stable initial-Li-free anode. To show the generality of using Li alloys to regulate Li deposition with good electro-mechanical stability, we also successfully conducted the studies of Zn, Al and Sb interphase on Cu foils for Li metal plating/cycling, and improved electrochemical reversibility were also realized.

2. Experimental

2.1. Materials preparation

Metallic Sn, Zn, Al, and Sb nanolayers coated Cu foils with controlled thickness were fabricated using magnetron-sputtering, which were labeled as Cu/S-Sn, Cu/S-Zn, Cu/S-Al and Cu/S-Sb electrodes, respectively. Before electrode fabrication, Cu foil was cleaned with 20% acetone solution and then 1% HNO_3 to remove the native oxide layer. A slurry process was adopted to prepare a Sn particle coating layer on Cu foil (Cu/C-Sn) with average active mass loading of ~0.06 mg cm^{-2}, which consisted with 92wt% Sn powder (<1 μm) and 8wt% lithium polyacrylate (LiPAA). Li rich Mn-based cathode (LRM) was purchased from Guangdong Canrd New Energy Technology Co., Ltd. A slurry with 80 wt% LRM active materials, 10 wt% carbon black and 10 wt% Polyvinylidene fluoride (PVDF) was adopted to prepare LRM electrode with average active mass loading of ~10.0 mg cm^{-2}.

2.2. Materials characterization

Scanning electron microscope (SEM, Nova NanoSEM 450) was used to investigate the structure and morphology of the as-prepared electrodes before and after Li plating/stripping cycling. Electron probe microanalysis (EPMA, EPMA-8050-G) was conducted to identify the elemental information and distribution of samples.

2.3. Electrochemical testing

Electrochemical performance was tested using the coin cell configuration using polypropylene as the separator. The electrolyte was 1 M $LiPF_6$ in mixed solvents of ethylene carbonate (EC) and dimethyl carbonate (DEC) (1:1 in volume) with 5 wt% fluoroethylene carbonate (FEC) as additives, unless otherwise stated. Cyclic voltammetry (CV) and electrochemical impedance spectrum (EIS) tests were performed on Biologic VMP3 electrochemical workstation. CV for Li||Cu/S-Sn and Li||Cu cell was conducted at a scanning rate of 0.01 mV S^{-1} with the voltage from 0.01 V to 1.5 V. EIS was conducted with the frequency from 100 mHz to 100 kHz. Initial Coulombic efficiency was tested by plating Li on substrates at 0.1 mA cm^{-2} for 10 h followed by stripping Li with the cut-off voltage of 1.0 V. Coulombic efficiency for Li plating/stripping cycling was tested in Li||Cu cells. Before electrochemical measurement, the electrodes were pre-cycled between 0 V and 0.5 V for 5 cycles at 50 μA for activation. The cells were then cycled by discharging for 1 h and charging to 1.0 V at 1 mA cm^{-2}. The electrodes used in anode-free batteries were also electrochemically activated using the same procedure in half cells. Anode-free cells with LRM cathodes were activated at 0.1 C (1 C = 200 mAh g^{-1}) and then cycled at 0.2 C with potential range from 2.0 to 4.8 V. The electrolyte for anode-free full cells was 1 M $LiPF_6$ in FEC/3, 3, 3-fluoroethylmethyl carbonate (FEMC)/1, 1, 2, 2-tetrafluoroethyl-2′, 2′, 2′-trifluororoethylether (HFE) with a weight ratio of 2: 6: 2.

2.4. Density function theory (DFT) calculation

The DFT calculations were performed with Vienna Ab initio Simulation Package (VASP) code [29]. The Perdew-Burke-Ernzerhof (PBE) was applied to approximate the exchange-correlation functional. The projector augmented wave (PAW) method was used for electron and core interaction [30–32]. The $Li_{22}Sn_5$ (352Li, 80Sn) and Cu (256Cu) bulk structures were constructed. A cut-off energy of 400 eV was used for all calculations. The convergence criteria for electronic relaxation was 10^{-5} eV and the convergence criteria for ionic relaxation was set to be 0.01 eV/Å, respectively. All structures were fully relaxed and reached the required accuracy. The (100), (110) and (111) surface orientations were considered for surface energy calculation of $Li_{22}Sn_5$ and Cu. All slab structures were constructed by using material studio. The surface energy "γ" was defined as follows [33]:

$$\gamma = \left(E_{slab} - E_{bulk}\right)/2A$$

Where E_{slab} is the total energy of the slab structure, E_{bulk} is the total energy of the bulk structure and A is the surface area. Based on the lowest surface energy of $Li_{22}Sn_5$, and Cu, the corresponding surface orientations were used for binding energy calculation. The binding energy of $Li_{22}Sn_5$ and Cu with one Li atom binding on the surface were calculated. The binding energy E_b was described as follows [34]:

$$E_b = E_{sub+Li} - \left(E_{sub} + E_{Li}\right)$$

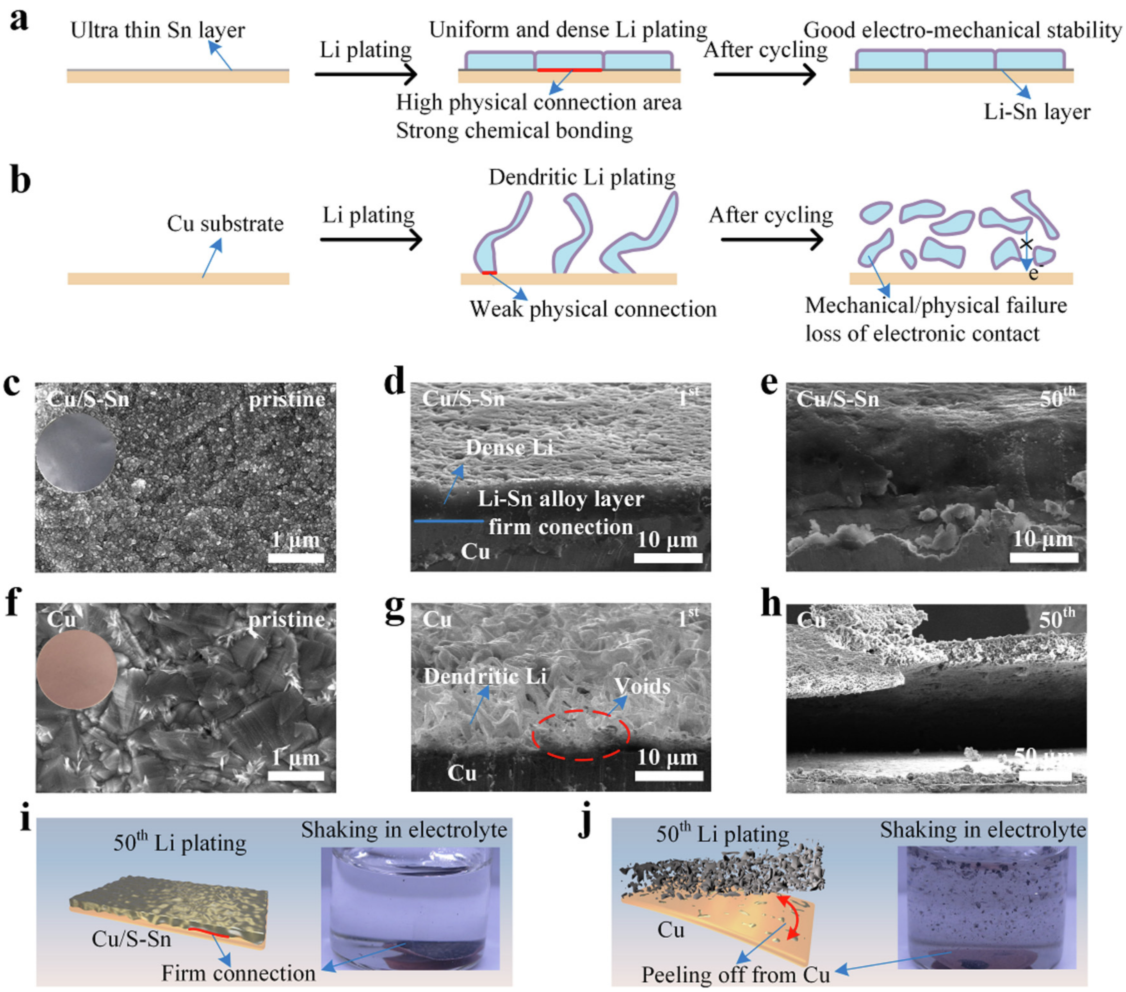

Fig. 1. Schematic diagram of the initial Li plating process and the evolutions of the morphology and structure of the (a) Cu/S-Sn and (b) Cu electrodes on cycling. Top-view SEM images of the (c) pristine Cu/S-Sn and (f) Cu electrodes. The inserts were the corresponding digital photos. Cross-section SEM images of the (d) Cu/S-Sn and (g) Cu electrodes after the 1st Li plating. Cross-section SEM images of the (e) Cu/S-Sn and (h) Cu electrodes after the 50th Li plating. Schematic diagrams of the evolution of (i, left) Cu/S-Sn and (j, left) Cu electrodes on cycling. The digital photos of the (i, right) Cu/S-Sn and (j, right) bare Cu electrodes at the 50th Li plating after shaking in electrolyte for 5 s. The test was conducted after Li plating at 1 mA cm^{-2} for 1 h followed by charging to 1 V at same current density to make Li strip for each cycle.

Where E_{sub+Li} is the total energy of the slab structure bonding with one Li, E_{sub} is the total energy of surface structure, and E_{Li} is the total energy of one Li.

Interface diffusion of Li and $Li_{22}Sn_5$ layers: The Li/$Li_{22}Sn_5$ interface structure was created by binding the four Li layers and seven $Li_{22}Sn_5$ layers together, in which four Li layers consisted 128Li and seven $Li_{22}Sn_5$ layers included 176Li, 40Sn. The ab initio molecular dynamic simulation was performed to study the atomic interface diffusion of Li/$Li_{22}Sn_5$ structure. The atoms on the Li/$Li_{22}Sn_5$ interface tended to mix together, which formed the atoms mixing region between Li and $Li_{22}Sn_5$ layer and the height of the atoms mixing region was around 1.85 Å. Besides, the total energy of initial and final Li/$Li_{22}Sn_5$ structures were compared. The initial and final Li/$Li_{22}Sn_5$ structure were −742.27 eV and −755.12 eV, which indicated that the Li/$Li_{22}Sn_5$ structure was energetic preference from initial Li/$Li_{22}Sn_5$ structure to final Li/$Li_{22}Sn_5$ structure with atoms mixing region.

The Li/$Li_{22}Sn_5$ interface structure was created by binding the four Li layers and seven $Li_{22}Sn_5$ layers together, in which four Li layers consisted 128Li and seven $Li_{22}Sn_5$ layers included 176Li and 40Sn. The ab initio molecular dynamic simulation was performed to study the atomic interface diffusion of Li/$Li_{22}Sn_5$ structure. The atoms on the Li/$Li_{22}Sn_5$ interface tended to mix together, which formed the atoms mixing region between Li and $Li_{22}Sn_5$ layer and the height of the atoms mixing region was around 1.85 Å. Besides, the total energy of initial and final Li/$Li_{22}Sn_5$ structures were compared. The initial and final Li/$Li_{22}Sn_5$ structure were −742.27 eV and −755.12 eV, which indicated that the Li/$Li_{22}Sn_5$ structure was energetic preference from initial Li/$Li_{22}Sn_5$ structure to final Li/$Li_{22}Sn_5$ structure with atoms mixing region.

3. Results and discussion

Fig. 1a, b schematically illustrated the initial Li deposition processes and the evolutions after cycling on Cu current collectors with and without a uniform Sn coating nanolayer fabricated through a magnetron-sputtering method (denoted as Cu/S-Sn foil and Cu foil), respectively. For the Cu/S-Sn foil, the ultrathin Sn layer is first electrochemical lithiated to form Li-Sn alloy ($Li_{22}Sn_5$ for complete reaction), which is lithiophilic, and delivers low Li nucleation energy barrier [35,36]. Importantly, the phase of $Li_{22}Sn_5$ would not take in more Li and its structure would remain stable during the subsequent Li plating/stripping, and thus could enable in planar deposition of metallic Li with good electro-mechanical stability. Due to the large lattice difference of Li and Cu, Li shows huge energy barrier for nucleation and growth on Cu surface [37,38]. Dendritic Li tends to form and expand, causing large accessible surface area to organic electrolyte and severe side reactions between them. During the subsequent cycling processes, Li dendrites dissolve and reform, and their whisker and porous morphology is likely to lose electronic connection at the root of some Li dendrites during their dissolution, leading to the accumulation of residual inactive metallic Li and the formation of porous Li layer [1,39].

The morphology and structure of the deposited Li on Cu/S-Sn and Cu electrodes were investigated by SEM. Top-view SEM images of Cu/S-Sn foil (Fig. 1c) showed smooth surface with dense and uniformly distributed Sn nanoparticles (<100 nm), in sharp contrast of the initial rough surface of Cu foil (Fig. 1f). The inserted digital photos showed the initial golden yellow of Cu foil turned gray after sputtering, suggesting the successful formation of Sn surface layer on Cu substrate. The Cu/S-Sn electrode possessed uniform and compact initial Li deposition layer after plating 1 mAh cm^{-2} of metallic Li (Fig. 1d), in sharp contrast to the dendritic Li deposits on the bare Cu electrode (Fig. 1g). The thickness of the Li deposition layer on Cu/S-Sn electrode was about 5 μm, close to the theoretical thickness of a completely dense Li metal layer with an area capacity of 1 mAh cm^{-2}, while the thickness of Li deposits reached over 10 μm for the bare Cu electrode, indicating their porous structure. Top-view SEM images showed smooth surface of the Li deposits after 10 Li plating/stripping cycles (**Fig. S4**a), which was very different from the mossy Li deposits on the bare Cu electrode (**Fig. S4**b). With the Li plating/stripping cycle number increasing to 50, flat Li deposition layer was still maintained for the Cu/S-Sn electrode (Fig. 1e). In contrast, a loose and porous Li structure was observed for the bare Cu foil electrode due to the dendrite Li expansion, and inactive metallic Li and SEI accumulation (Fig. 1h). Even after 150 cycles, planar Li deposition layer with dense structure was still achieved for the Cu/S-Sn electrode, revealing the superior structural stability of the Cu/S-Sn electrode (**Fig. S5**). The cross-section SEM images further revealed the stable structure of deposited metallic Li layer on Cu/S-Sn electrode. It firmly connected with the current collector and remained dense without obvious avoids after the 10th (Fig. **S6**a) and 50th Li plating (Fig. 1e), which was strongly related with the in-planar Li deposition behavior and the strong binding between the metallic Li and Li-Sn alloy interphase on current collector. In sharp contrast, the cross-section SEM images showed that there existed large abundant avoids or even gaps between the Cu current collectors and the deposited layer in the observed area (**Figs. S6**b, 1h). These results indicated the poor electro-mechanical stability of the metallic Li plating on the Cu electrode. It caused the loss of mechanical and electronic connection between the active layer and current collector, which lead to fast electrochemical failure as well.

We further compared the mechanical stability of the Li deposits on Cu/S-Sn and Cu current collectors to support the robust planar Li deposition on Cu/S-Sn substrates. Fig. 1i, left and j, left schematically showed the morphologies and structures of Li deposits on Cu/S-Sn and Cu current collectors, respectively. Compact in-planar Li deposits with strong binding with the current collector would help to realize close connection with the current collector, suppress the increase in impedance, and reduce the risk of the loss of electronic contact, which support highly reversible Li plating/stripping cycling. In contrast, repeated dendritic Li growth and its incomplete dissolution would lead to fast accumulation of inactive Li, and the formation of porous and loose Li layers with weak connection with the bare Cu substrate, which would easily lead to the loss of electronic contact between the deposited metallic Li and the substrate, and even their complete separation. Experimentally, the Cu/S-Sn electrodes with 1 mAh cm^{-2} Li plating after different cycles were taken out from the cells and rested in electrolyte. After mechanical shaking, the electrolyte with the Cu/S-Sn electrode after the 10th (**Fig. S7**a, b) and 50th (Fig. 1i, right) cycle-Li plating remained clear, and no shedding metallic Li was observed in the electrolyte, which strongly supported the good electro-mechanical stability of the Cu/S-Sn electrodes. Such electro-mechanical stability on cycling was beneficial for reducing the accumulation of inactive Li on cycling, which supported the high Coulombic efficiency of Cu/S-Sn electrode. In sharp contrast, the deposited metallic Li on the Cu current collector showed fast separation with the substrate in electrolyte after shaking. The electrolyte with the electrode after the 10th-cycle Li plating became turbid (**Fig. S7**c, d), and the situation become even worse after the 50th cycle (Fig. 1j, right). The electrolyte turned turbid completely and large gray/black deposits were dispersed in the entire suspension after immersion of the Cu electrode without shaking, and the deposits were fully peeled after 5 s-mechanical shaking. Thus, the planer Li plating behavior and its firm connection with the current collector enabled long-term electro-mechanical stability, which became one of the main reason for the enhanced electrochemical performance of the Cu/S-Sn electrode. The good electro-mechanical stability of Cu/S-Sn electrode on Li plating/stripping cycling ensured the high utilization of active Li and reduced the accumulation of thick inactive and porous Li layer on electrode, giving great potential for the inhibition of cell failure. **Fig. S8** showed the EIS results of the Li||Cu/S-Sn and Li||Cu cells after the 1st and 50th Li plating cycles. The Li||Cu/S-Sn cell delivered much lower interface impedance (~24 and 27 ohms at the 1st and 50th Li plating, respectively) than that of the Li||Cu cells (~38 and 45 ohms at the 1st and 50th Li plating, respectively). This result supported the reduced side reactions and suppressed inactive Li formation due to the introduction of Cu/S-Sn electrode.

The Coulombic efficiency for the initial Li plating/stripping cycle was tested to show the enhanced electrochemical performance for Cu/S-Sn foil electrode in half-cell configuration (**Fig. S9**). The value of initial Coulombic efficiency of the Cu/S-Sn electrode reached as high as 97.1% in carbonate electrolyte, much high than 93.5% for that of the bare Cu electrode counterpart. The Coulombic efficiency measurement on cycling was conducted to show the advancement of Li-Sn alloy interphase layer of Cu/S-Sn electrode in improving the electrochemical Li plating/stripping reversibility. The results showed that Cu/S-Sn electrode not only delivered much longer lifespan (Fig. 2a) but also possessed higher Coulombic efficiency on cycling (insert in Fig. 2a) in comparison to bare Cu electrode. Stable Li plating/stripping cycling with average Coulombic efficiency of 94.1% for 400 cycles was realized for the Cu/S-Sn electrode at 1 mA cm^{-2} and 1 mAh cm^{-2} in carbonate electrolyte, while the bare Cu electrode showed much lower average Coulombic efficiency of 82.4% and it failed within 70 cycles under the same test conditions. The results of Coulombic efficiency tested at 1 mA cm^{-2} and 3 mAh cm^{-2} (**Fig. S10**), and 2 mA cm^{-2} and 2 mAh cm^{-2} (**Fig. S11**) also supported the significantly improved cycling stability and highly reversible Li plating/stripping cycling of the Cu/S-Sn electrode in different test conditions.

The rate capability of Cu/S-Sn electrode was also conducted at different current density and area capacity conditions. With fixed deposited Li capacity of 1 mAh cm^{-2}, Cu/S-Sn electrode delivered highly stable cycling behavior at different current densities (0.5, 1, 2, 3, and 0.5 mA cm^{-2} for every 30 cycles), and exhibited high Coulombic efficiency above 91% for all the current conditions (**Fig. S12**). Instead, bare Cu electrode showed lower average Coulombic efficiency and fast failure in less than 100 cycles (Fig. 2b). Moreover, large fluctuation in values of Coulombic efficiency from 91.7% to 84.0% was observed for the Cu foil electrode on cycling tested at 2 mA cm^{-2}, in sharp contrast to the stable values with small change from 95.2% to 93.5% for the Cu/S-Sn electrode, indicating the much improved stability and reversibility of the Cu/S-Sn electrode. The voltage profiles in Fig. 2c showed the every-increasing voltage polarization of Li||Cu cells during cycling, indicating the increased impedance caused by the deteriorated electro-mechanical stability and accumulated Li loss. The Cu/S-Sn electrode also showed advancement in electrochemical measurement at different area capacities (0.5, 1, 2, 3, 0.5 mAh cm^{-2}) with fixed current density of 1 mA cm^{-2} (**Fig. 2**d). It showed stable Columbic efficiency with average value of as high as ~95.0% at different fixed areal capacity for each 30 cycles (**Fig. S13**). As comparison, the values of Coulombic efficiency for the Cu electrode started to decrease quickly when the areal capacity switched to 3 mAh cm^{-2}, and dropped to ~0% in 30 cycles. When the current density returned to 0.5 mAh cm^{-2}, the value remained at 0% and could not

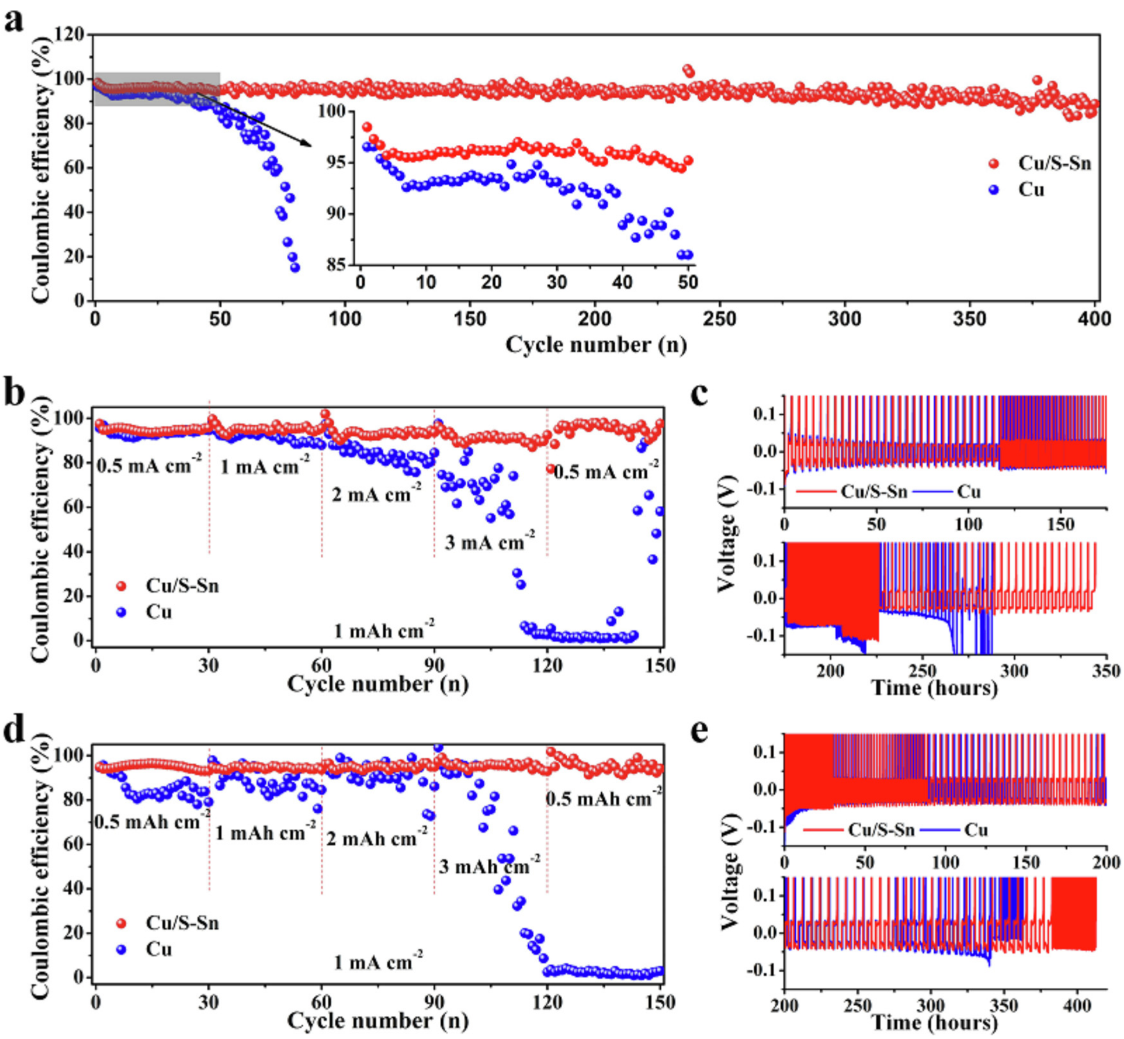

Fig. 2. (a) Plots of Coulombic efficiency of Li||Cu/S-Sn and Li||Cu cells. The tests were conducted via plating Li on Cu/S-Sn and Cu substrates at 1 mA cm^{-2} for 1 h followed by charging to 1 V at same current density for each cycle. (b) Columbic efficiency of Cu/S-Sn and Cu electrodes cycled with Li plating capacity of 1 mAh cm^{-2} and different current densities (0.5, 1, 2, 3 and 0.5 mA cm^{-2}) , and (c) the corresponding voltage profiles with time. (d) Columbic efficiency of Cu/S-Sn and Cu electrodes cycled at current density of 1 mA cm^{-2} and different Li plating capacities (0.5, 1, 2, 3 and 0.5 mAh cm^{-2}), and (e) the corresponding voltage profiles with time. The cells were cycled for 30 cycles at each current density condition and areal capacity condition, respectively.

be recovered to a high value, indicating the complete failure of the bare Cu electrode. The voltage profiles of the Cu/S-Sn electrode and the bare Cu electrode were shown in Fig. 2e. Stable voltage profiles with low polarization were observed for the Cu/S-Sn electrode during the full cycle operations under different areal capacities conditions, while the obvious increase of polarization and short-circuit occurred for the bare Cu electrode with cycling. These results indicate the great advancement of using Cu/S-Sn foil electrode to reduce active Li loss and improve the electrochemical performance in high-energy-density LMBs systems.

The electro-mechanical stability of the Cu/S-Sn electrode and the related mechanism behind were further investigated using both experiment and theoretical simulation. The nucleation overpotential is defined as the value for the voltage difference between the bottom of voltage dip and the Li plating flat, which is an important parameter for the evaluation of current collectors for Li plating. At different current densities of 0.01 (**Fig. S14**), 0.1 (**Fig. S15**) and 3 mA cm^{-2} (**Fig. S16**), the Cu/S-Sn electrode delivered significantly reduced Li nucleation overpotential in compared to the bare Cu electrode counterpart (Fig. 3a). The small Li nucleation overpotential arose from the lithiophilic nature and low nucleation energy barrier of Li-Sn alloy, which was critical for the subsequent Li plating/stripping cycling [40,41]. The cyclic voltammetry (CV) curves of Li||Cu/S-Sn cell (Fig. 3b) clearly revealed the alloying reaction of Sn during the cathodic scan. The reduction peaks at ~0.39 V suggested the formation of $Li_{22}Sn_5$ phase before Li metal plating [42]. As comparison, Li||Cu cell only showed broad peaks between ~0.56 and ~0.90 V, corresponding to the formation of SEI and the reduction of oxidation layer on the Cu foil surface (Fig. 3c) [43]. The simulation results showed that Li diffusion into $Li_{22}Sn_5$ layer tended to occur at the contact interface (Fig. 3d–f), indicating good affinity between the deposited metallic Li and the Li-Sn alloy substrate.

We further conducted the calculations of binding energy between Li and $Li_{22}Sn_5$ (Fig. 3g, j), and between Li and Cu (Fig. 3h, k). The calculated binding energy was −0.53 eV between Li and $Li_{22}Sn_5$, in sharp comparison to 0.18 eV for that between Li and Cu. These results supported the preferential deposition of metallic Li on Li-Sn substrate rather than Cu substrate, in agreement with the lower Li nucleation energy barrier of Li-Sn substrate than bare Cu substrate [35,44]. These calculated results were confirmed by electrochemical Li deposition experiments, which were carried out by plating Li on a Cu mesh coated with S-Sn on Cu foil substrates (**Fig. S17**). With a low area capacity of 0.1 mAh cm^{-2} (Fig. 3i), electrode with ultrathin Sn layer showed a dispersive distribution of deposited Li on the skeleton and no metallic Li deposits were

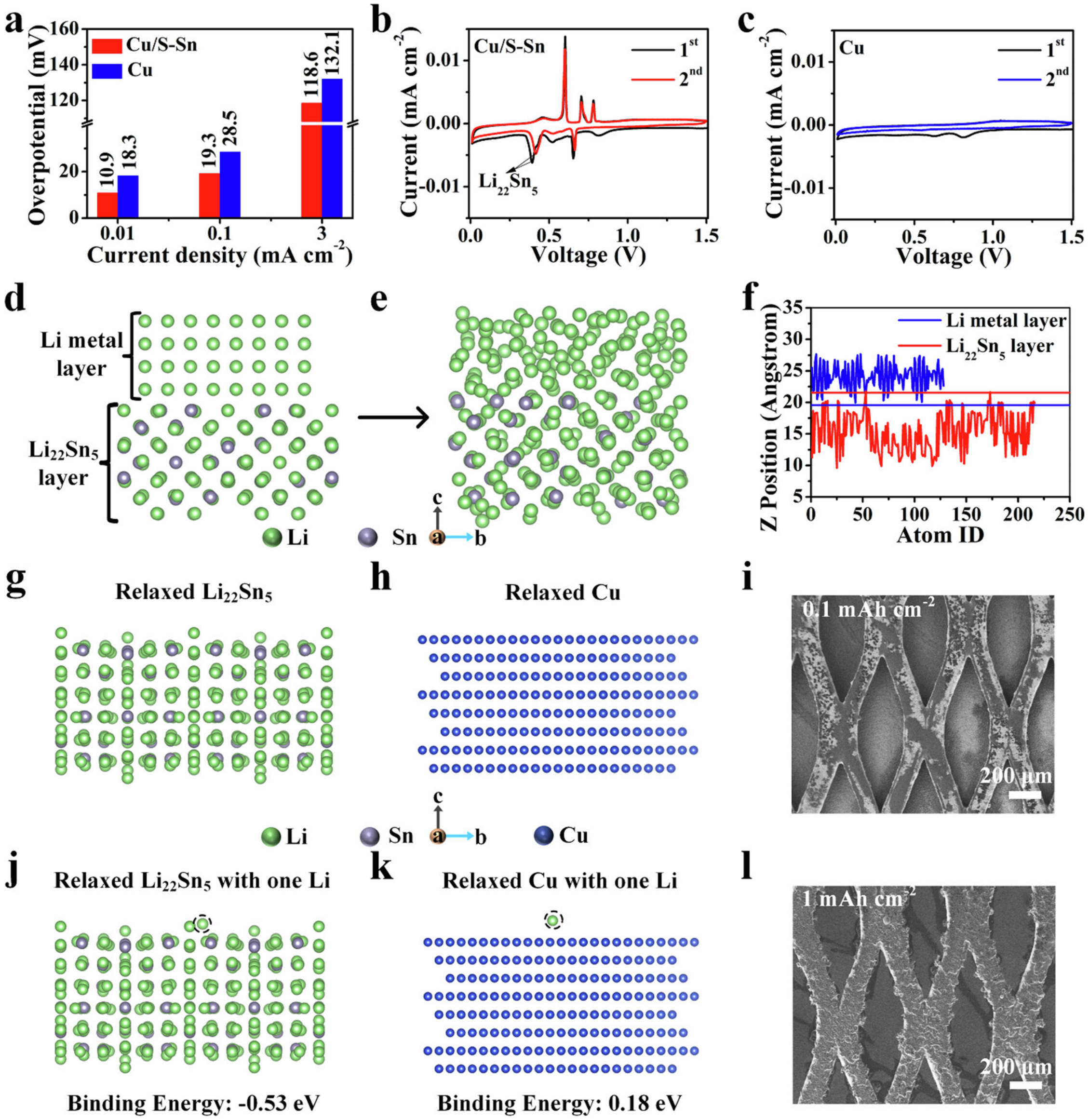

Fig. 3. (a) Comparison of the Li nucleation overpotential on Cu/S-Sn and Cu electrodes at different current densities. (b, c) CV results of the Li||Cu/S-Sn and Li||Cu cells, respectively. (d-f) Simulation results of the interface diffusion between Li metal layer and $Li_{22}Sn_5$ layer. (g, j) Calculation results of binding energy between Li and $Li_{22}Sn_5$. (h, k) Calculation results of binding energy between Li and Cu. (i) SEM images of electrodes of Cu mesh with S-Sn on Cu foil after plating of 0.1 and (l) 1 mAh cm^{-2} Li at 0.1 mA cm^{-2}.

observed on the bottom Cu substrate, showing the preferred Li plating on Li-Sn substrate. With the increase of area capacity to 1 mAh cm^{-2}, increased amount of Li deposits were observed on the skeleton of the Cu mesh with ultrathin Sn layer, and the Cu foil substrate kept Li free (Fig. 3l). In contrast, Li was randomly plated on both the Cu foil substrate and the skeleton of the Cu mesh for the electrode consisting of Cu mesh on Cu foil electrode (**Fig. S18**). The preferential deposition of metallic Li on the Sn-coated Cu skeleton rather than the bare Cu substrate further verified the superiority of Sn (Li-Sn) layer for regulating the lithium plating/stripping behavior in LMB systems. As probed above, the Cu foil electrode with Sn layer possessed reduced Li nucleation barrier and Li tended to be deposited on the Sn modified surface with good mechanical connection, which would be helpful for suppressing dendritic Li growth and reducing Li loss during Li plating/stripping cycling, and improve the lifespan of batteries.

Cu/S-Sn electrode delivered planar Li deposition morphology with good connection with the current collector and highly reversible Li plating/stripping behavior, showing great potential for high-energy-density LMBs. To reduce the cost and make good compatibility with the existing industrial application, we fabricated Sn coated Cu foil electrode via a slurry processing approach (Fig. 4a) with an ultralow Sn mass loading of 0.06 mg cm^{-2} (defined as Cu/C-Sn, **Figs. S19** and **S20**). As expected, the Cu/C-Sn electrodes shared similar electrochemical characteristics for Li electrochemical plating/stripping behavior with the Cu/S-Sn electrode. It delivered low Li nucleation overpotential of ~8.0 mV during the initial Li deposition processes (**Fig. S21**) in comparison to 18.3 mV for the bare Cu foil electrode at the same test conditions (**Fig. S14**b). Also, the Li deposits on the Cu/C-Sn electrode were chunky and compact, without producing undesirable dendritic Li (**Fig. S22**). During the electrochemical Li plating/stripping cycling, the Cu/C-Sn electrode delivered high average Coulombic efficiency of 95.4% for 250 cycles (Fig. 4b) at 1 mA cm^{-2} and 1 mAh cm^{-2}, showing the generality of using Sn species in improving the electrochemical Li plating/stripping behavior. Besides, the fabrication of Sn-particle coating layer was robust for using different commercial binders and they shared similar electrochemical behaviors for the as-achieved Cu/C-Sn electrodes (**Figs. S23–25**). Better cycling

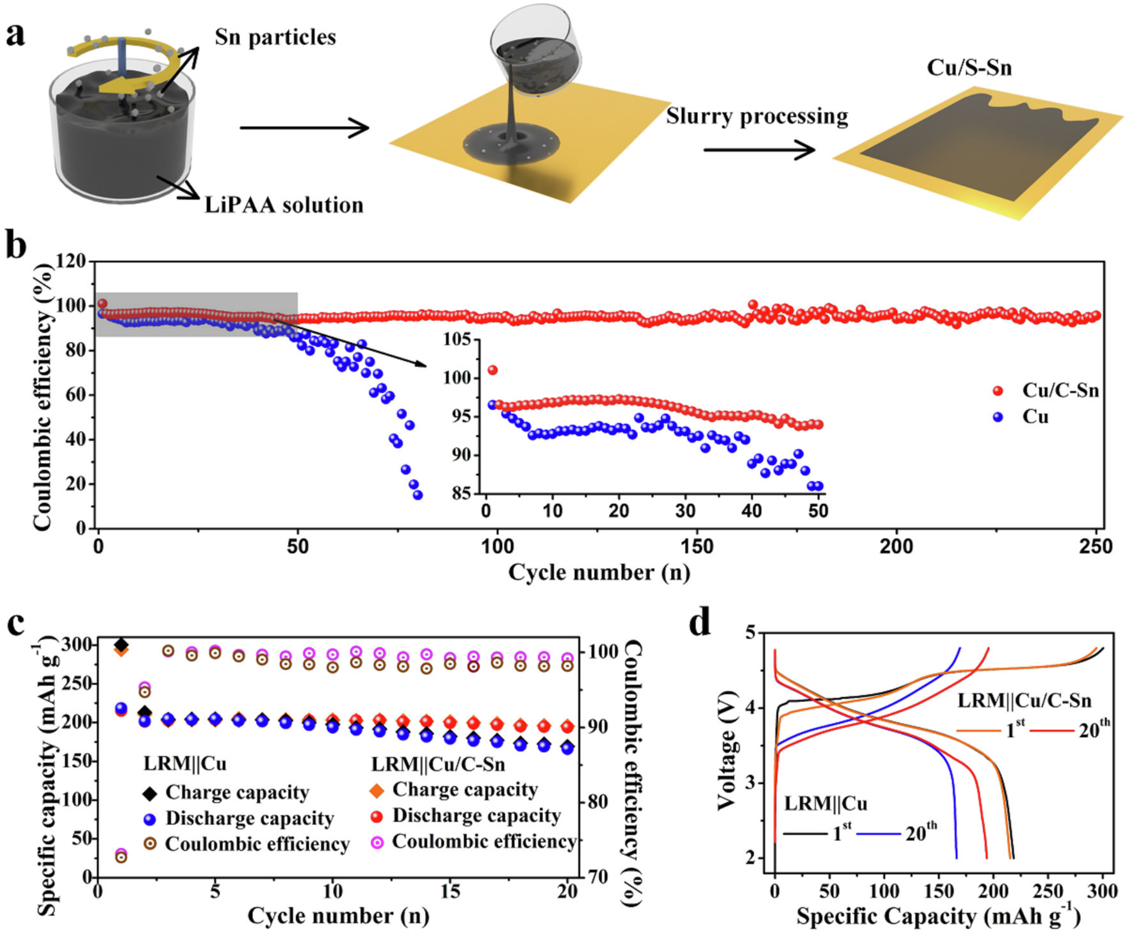

Fig. 4. (a) The schematic diagram of the fabrication of Cu/C-Sn electrode using a slurry approach. (b) Comparison of Coulombic efficiency-cycle number plots of Li||Cu/C-Sn and Li||Cu cells. The test was conducted with plating Li on Cu/C-Sn substrate at 1 mA cm^{-2} for 1 h followed by charging to 1 V at same current density for each cycle. (c) Electrochemical performance of LRM||Cu/C-Sn and LRM||Cu cells. The cells were activated at 0.1 *C* (1 *C* = 200 mAh g^{-1}) for the 1st cycle and then cycled at 0.2 *C* for the following cycles with the cutoff potential range between 2.0 and 4.8 V. (d) The specific capacity-voltage profiles of LRM||Cu/C-Sn and LRM||Cu cells at the 1st and 20th cycle.

stability could be achieved by further optimization for the size of Sn particles, slurry viscosity, and the binder species. Similar with the Cu/S-Sn electrode, the Cu/C-Sn electrode also showed uniform Li deposition morphology with long-term cycling (**Figs. S26** and **S27**), revealing the successful extension of using such a slurry coating approach for improving the Li plating/stripping cycling.

Based on the evaluation of using Sn (Li-Sn) containing substrates for electrochemical Li plating/stripping cycling, its application in anode-free batteries was further explored. Li rich Mn-based cathode (LRM) showed great potential in the application of high energy density batteries due to its high reversible capacity and considerable cycling stability at high charge cut-off voltage. LRM||Cu/C-Sn cell delivered similar capacity (201.2 mAh g^{-1}) to that of the LRM||Cu cell (201.8 mAh g^{-1}) for the 1st cycle and showed 16.7% higher capacity after 20 cycles. Also, the LRM||Cu/C-Sn cell delivered average Coulombic efficiency of 99.4% in comparison to the LRM||Cu cell (98.5%, Fig. 4c). The specific-capacity curves of the LRM||Cu/C-Sn cell and LRM||Cu cell were compared (Fig. 4d). The LRM||Cu/C-Sn delivered lower voltage polarization at the 1st and 20th cycles than that of the LRM||Cu cell, indicating the significantly enhanced electrochemical reversibility for the Cu/C-Sn electrode.

It is revealed that Li-Sn (Sn) could enable good electro-mechanical stability and highly reversible Li plating/stripping cycling, which features low nucleation overpotential of metallic Li and planar Li deposition behavior with good connection with the substrates. With no solubility in Li, the Li-Sn alloy functions as stable interphase that regulates electrochemical Li deposition. Based on the understanding of Li-Sn alloy for electrochemical Li plating/stripping, we believe that reversible and stable Li plating/stripping cycling could also be achieved in some other Li-M alloy containing substrates, which possess no or lower solubility in Li. Experimentally, Cu/S-Zn, Cu/S-Al and Cu/S-Sb electrodes delivered lower Li nucleation overpotential, suppressed Li dendrite formation and stable electrochemical Li plating/stripping cycling (**Figs. S28-S31**).

In summary, we have revealed that electro-mechanical stability plays important role in electrochemical cycling of initial-Li-free anode, and Li-Sn alloy (Sn) containing substrates could regulate the Li plating/stripping behaviors, and enable good electro-mechanical stability on cycling. Experimentally, we fabricated a Cu/C-Sn electrode through a facile slurry coating approach for anode-free battery systems. Compared with bare Cu, Li-Sn substrate delivered lower Li nucleation energy barrier, good affinity and higher binding energy with Li. During Li plating, uniform and dense Li deposits forms, which is close contact with the current collector formed, which significantly suppressed the side reactions, and enhanced the electrochemical reversibility. Furthermore, other metal elements (Zn, Al and Sb) for metallic Li plating/stripping, which could alloy with Li and possess no or lower solubility in Li, were also investigated and enhanced electrochemical reversibility was also realized.

Declaration of Competing Interest

The authors declare no competing financial interest.

CRediT authorship contribution statement

Xiancheng Wang: Investigation, Data curation, Writing – original draft. **Yufang He:** Data curation. **Shuibin Tu:** Data curation, Methodology. **Lin Fu:** Data curation, Methodology. **Zihe Chen:** Data curation. **Shiyu Liu:** Investigation. **Zhao Cai:** Investigation. **Li Wang:** Investigation. **Xiangming He:** Investigation. **Yongming Sun:** Supervision, Conceptualization, Methodology, Writing – review & editing.

Acknowledgments

The authors would like to thank the support by National Natural Science Foundation of China (No. 52072137). The authors would like to thank the Analytical and Testing Center of Huazhong University of Science and Technology for providing the facilities to conduct the characterization. The authors would like to thank the Optoelectronic Micro&Nano Fabrication and Characterizing Facility of Huazhong University of Science and Technology for the providing the facilities of materials synthesis.

Supplementary materials

Supplementary material associated with this article can be found, in the online version, at doi:10.1016/j.ensm.2022.04.009.

Reference

[1] C. Fang, J. Li, M. Zhang, Y. Zhang, F. Yang, J.Z. Lee, M.H. Lee, J. Alvarado, M.A. Schroeder, Y. Yang, B. Lu, N. Williams, M. Ceja, L. Yang, M. Cai, J. Gu, K. Xu, X. Wang, Y.S. Meng, Quantifying inactive lithium in lithium metal batteries, Nature 572 (2019) 511–515, doi:10.1038/s41586-019-1481-z.

[2] C. Niu, H. Pan, W. Xu, J. Xiao, J.G. Zhang, L. Luo, C. Wang, D. Mei, J. Meng, X. Wang, Z. Liu, L. Mai, J. Liu, Self-smoothing anode for achieving high-energy lithium metal batteries under realistic conditions, Nat. Nanotechnol. 14 (2019) 594–601, doi:10.1038/s41565-019-0427-9.

[3] X. Wu, W. Zhang, N. Wu, S.S. Pang, Y. Ding, G. He, Structural evolution upon delithiation/lithiation in prelithiated foil anodes–A case study of AgLi alloys with high Li utilization and marginal volume variation, Adv. Energy Mater. 11 (2021) 2003082, doi:10.1002/aenm.202003082.

[4] Y.H. Tan, G.X. Lu, J.H. Zheng, F. Zhou, M. Chen, T. Ma, L.L. Lu, Y.H. Song, Y. Guan, J. Wang, Z. Liang, W.S. Xu, Y. Zhang, X. Tao, H.B. Yao, Lithium fluoride in electrolyte for stable and safe lithium-metal batteries, Adv. Mater. 33 (2021) 2102134, doi:10.1002/adma.202102134.

[5] H. Chen, Y. Yang, D.T. Boyle, Y.K. Jeong, R. Xu, L.S. de Vasconcelos, Z. Huang, H. Wang, H. Wang, W. Huang, H. Li, J. Wang, H. Gu, R. Matsumoto, K. Motohashi, Y. Nakayama, K. Zhao, Y. Cui, Free-standing ultrathin lithium metal–graphene oxide host foils with controllable thickness for lithium batteries, Nat. Energy 6 (2021) 790–798, doi:10.1038/s41560-021-00833-6.

[6] J. Gao, C. Chen, Q. Dong, J. Dai, Y. Yao, T. Li, A. Rundlett, R. Wang, C. Wang, L. Hu, Stamping flexible Li alloy anodes, Adv. Mater. 33 (2021) 2005305, doi:10.1002/adma.202005305.

[7] Y. Qiao, H. Yang, Z. Chang, H. Deng, X. Li, H. Zhou, A high-energy-density and long-life initial-anode-free lithium battery enabled by a Li_2O sacrificial agent, Nat. Energy 6 (2021) 653–662, doi:10.1038/s41560-021-00839-0.

[8] S. Nanda, A. Gupta, A. Manthiram, Anode-free full cells–A pathway to high-energy density lithium-metal batteries, Adv. Energy Mater. 11 (2020) 2000804, doi:10.1002/aenm.202000804.

[9] Y. Tian, Y. An, C. Wei, H. Jiang, S. Xiong, J. Feng, Y. Qian, Recently advances and perspectives of anode-free rechargeable batteries, Nano Energy 78 (2020) 105344, doi:10.1016/j.nanoen.2020.105344.

[10] D. Wang, Y. Liu, G. Li, C. Qin, L. Huang, Y. Wu, Liquid metal welding to suppress Li dendrite by equalized heat distribution, Adv. Funct. Mater. 31 (2021) 2106740, doi:10.1002/adfm.202106740.

[11] S. Liu, X. Zhang, R. Li, L. Gao, J. Luo, Dendrite-free Li metal anode by lowering deposition interface energy with $Cu_{99}Zn$ alloy coating, Energy Storage Mater. 14 (2018) 143–148, doi:10.1016/j.ensm.2018.03.004.

[12] Y. Lu, J. Wang, Y. Chen, X. Zheng, H. Yao, S. Mathur, Z. Hong, Spatially controlled lithium deposition on silver-nanocrystals-decorated TiO_2 nanotube arrays enabling ultrastable lithium metal anode, Adv. Funct. Mater. 31 (2020) 2009605, doi:10.1002/adfm.202009605.

[13] A. Hu, W. Chen, X. Du, Y. Hu, T. Lei, H. Wang, L. Xue, Y. Li, H. Sun, Y. Yan, J. Long, C. Shu, J. Zhu, B. Li, X. Wang, J. Xiong, An artificial hybrid interphase for an ultrahigh-rate and practical lithium metal anode, Energy Environ. Sci. 14 (2021) 4115–4124, doi:10.1039/d1ee00508a.

[14] R. Weber, M. Genovese, A.J. Louli, S. Hames, C. Martin, I.G. Hill, J.R. Dahn, Long cycle life and dendrite-free lithium morphology in anode-free lithium pouch cells enabled by a dual-salt liquid electrolyte, Nat. Energy 4 (2019) 683–689, doi:10.1038/s41560-019-0428-9.

[15] X. Ke, Y. Liang, L. Ou, H. Liu, Y. Chen, W. Wu, Y. Cheng, Z. Guo, Y. Lai, P. Liu, Z. Shi, Surface engineering of commercial Ni foams for stable Li metal anodes, Energy Storage Mater. 23 (2019) 547–555, doi:10.1016/j.ensm.2019.04.003.

[16] J. Chen, J. Xiang, X. Chen, L. Yuan, Z. Li, Y. Huang, Li_2S-based anode-free full batteries with modified Cu current collector, Energy Storage Mater. 30 (2020) 179–186, doi:10.1016/j.ensm.2020.05.009.

[17] C. Yan, X.B. Cheng, Y. Tian, X. Chen, X.Q. Zhang, W.J. Li, J.Q. Huang, Q. Zhang, Dual-layered film protected lithium metal anode to enable dendrite-free lithium deposition, Adv. Mater. 30 (2018) 1707629, doi:10.1002/adma.201707629.

[18] H.H. Weldeyohannes, L.H. Abrha, Y. Nikodimos, K.N. Shitaw, T.M. Hagos, C.-.J. Huang, C.-.H. Wang, S.-.H. Wu, W.-.N. Su, B.J. Hwang, Guiding lithium-ion flux to avoid cell's short circuit and extend cycle life for an anode-free lithium metal battery, J. Power Sources 506 (2021) 230204, doi:10.1016/j.jpowsour.2021.230204.

[19] O. Sheng, J. Zheng, Z. Ju, C. Jin, Y. Wang, M. Chen, J. Nai, T. Liu, W. Zhang, Y. Liu, X. Tao, In situ construction of a LiF-enriched interface for stable all-solid-state batteries and its origin revealed by cryo-TEM, Adv. Mater. 32 (2020) e2000223, doi:10.1002/adma.202000223.

[20] Z. Ju, C. Jin, H. Yuan, T. Yang, O. Sheng, T. Liu, Y. Liu, Y. Wang, F. Ma, W. Zhang, J. Nai, X. Tao, A fast-ion conducting interface enabled by aluminum silicate fibers for stable Li metal batteries, Chem. Eng. J. 408 (2021) 128016, doi:10.1016/j.cej.2020.128016.

[21] K. Yan, Z. Lu, H.-.W. Lee, F. Xiong, P.-.C. Hsu, Y. Li, J. Zhao, S. Chu, Y. Cui, Selective deposition and stable encapsulation of lithium through heterogeneous seeded growth, Nat. Energy 1 (2016) 16010, doi:10.1038/nenergy.2016.10.

[22] Z.T. Wondimkun, W.A. Tegegne, J. Shi-Kai, C.-.J. Huang, N.A. Sahalie, M.A. Weret, J.-.Y. Hsu, P.-.L. Hsieh, Y.-.S. Huang, S.-.H. Wu, W.-.N. Su, B.J. Hwang, Highly-lithiophilic Ag@PDA-GO film to suppress dendrite formation on Cu substrate in anode-free lithium metal batteries, Energy Storage Mater. 35 (2021) 334–344, doi:10.1016/j.ensm.2020.11.023.

[23] J. Duan, Y. Zheng, W. Luo, W. Wu, T. Wang, Y. Xie, S. Li, J. Li, Y. Huang, Is graphite lithiophobic or lithiophilic? Natl. Sci. Rev. 7 (2020) 1208–1217, doi:10.1093/nsr/nwz222.

[24] W. Wu, J. Duan, J. Wen, Y. Chen, X. Liu, L. Huang, Z. Wang, S. Deng, Y. Huang, W. Luo, A writable lithium metal ink, Sci. China Chem. 63 (2020) 1483–1489, doi:10.1007/s11426-020-9810-1.

[25] C.-.A. Lo, C.-.C. Chang, Y.-.W. Tsai, S.-.K. Jiang, B.J. Hwang, C.-.Y. Mou, H.-.L. Wu, Regulated Li electrodeposition behavior through mesoporous silica thin film in anode-free lithium metal batteries, ACS Appl. Energ. Mater. 4 (2021) 5132–5142, doi:10.1021/acsaem.1c00664.

[26] H. Kwon, J.H. Lee, Y. Roh, J. Baek, D.J. Shin, J.K. Yoon, H.J. Ha, J.Y. Kim, H.T. Kim, An electron-deficient carbon current collector for anode-free Li-metal batteries, Nat. Commun. 12 (2021) 5537, doi:10.1038/s41467-021-25848-1.

[27] Y. An, H. Fei, G. Zeng, X. Xu, L. Ci, B. Xi, S. Xiong, J. Feng, Y. Qian, Vacuum distillation derived 3D porous current collector for stable lithium–metal batteries, Nano Energy 47 (2018) 503–511, doi:10.1016/j.nanoen.2018.03.036.

[28] J. Qian, B.D. Adams, J. Zheng, W. Xu, W.A. Henderson, J. Wang, M.E. Bowden, S. Xu, J. Hu, J.-.G. Zhang, Anode-free rechargeable lithium metal batteries, Adv. Funct. Mater. 26 (2016) 7094–7102, doi:10.1002/adfm.201602353.

[29] J. Hafner, G. Kresse, The vienna AB-initio simulation program VASP–An efficient and versatile tool for studying the structural, dynamic, and electronic properties of materials, in: A. Meike; P. E. A. Turchi, (Eds.), Properties of Complex Inorganic Solids, Springer., US: Boston, MA, 1997, pp 69–82.

[30] K.B. John, P. Perdew, Matthias Ernzerhof, Generalized gradient approximation made simple, Phys. Rev. Lett. 77 (1996) 3865–3868, doi:10.1103/PhysRevLett.77.3865.

[31] G. Kresse, J. Furthmüller, Efficient iterative schemes for ab initio total-energy calculations using a plane-wave basis set, Phys. Rev. B 54 (1996) 11169–11186, doi:10.1103/PhysRevB.54.11169.

[32] G. Kresse, J. Furthmuller, Efficiency of ab-initio total energy calculations for metals and semiconductors using a plane-wave basisset, Comput. Mater. Sci. 6 (1996) 15–50, doi:10.1016/0927-0256(96)00008-0.

[33] Y. He, H. Pham, Y. Gao, R. Patel, S. Sarkar, X. Liang, J. Park, Lithium-ion batteries–Discovery of an unexpected metal dissolution of thin-coated cathode particles and its theoretical explanation, Adv. Theory Simul. 3 (2020) 2000002, doi:10.1002/adts.202070011.

[34] S. Li, J. Fu, G. Miao, S. Wang, W. Zhao, Z. Wu, Y. Zhang, X. Yang, Toward planar and dendrite-free Zn electrodepositions by regulating Sn-crystal textured surface, Adv. Mater. 33 (2021) 2008424, doi:10.1002/adma.202008424.

[35] J. Luan, Q. Zhang, H. Yuan, Z. Peng, Y. Tang, S. Wu, H. Wang, Sn layer decorated copper mesh with superior lithiophilicity for stable lithium metal anode, Chem. Eng. J. 395 (2020) 124922, doi:10.1016/j.cej.2020.124922.

[36] B. Han, D. Xu, S.S. Chi, D. He, Z. Zhang, L. Du, M. Gu, C. Wang, H. Meng, K. Xu, Z. Zheng, Y. Deng, 500 Wh kg^{-1} class Li metal battery enabled by a self-organized core-shell composite anode, Adv. Mater. 32 (2020) 2004793, doi:10.1002/adma.202004793.

[37] V. Pande, V. Viswanathan, Computational screening of current collectors for enabling anode-free lithium metal batteries, ACS Energy Lett. 4 (2019) 2952–2959, doi:10.1021/acsenergylett.9b02306.

[38] Z. Jiang, H.J. Guo, Z. Zeng, Z. Han, W. Hu, R. Wen, J. Xie, Reconfiguring organosulfur cathode by over-lithiation to enable ultrathick lithium metal anode toward practical lithium-sulfur batteries, ACS Nano 14 (2020) 13784–13793, doi:10.1021/acsnano.0c06133.

[39] Z.T. Wondimkun, T.T. Beyene, M.A. Weret, N.A. Sahalie, C.-.J. Huang, B. Thirumalraj, B.A. Jote, D. Wang, W.-.N. Su, C.-.H. Wang, G. Brunklaus, M. Winter, B.-.J. Hwang, Binder-free ultra-thin graphene oxide as an artificial solid electrolyte interphase for anode-free rechargeable lithium metal batteries, J. Power Sources 450 (2020) 227589, doi:10.1016/j.jpowsour.2019.227589.

[40] J. Chen, Q. Li, T.P. Pollard, X. Fan, O. Borodin, C. Wang, Electrolyte design for Li metal-free Li batteries, Mater. Today 39 (2020) 118–126, doi:10.1016/j.mattod.2020.04.004.

[41] P. Zhai, L. Liu, Y. Wei, J. Zuo, Z. Yang, Q. Chen, F. Zhao, X. Zhang, Y. Gong, Self-healing nucleation seeds induced long-term dendrite-free lithium metal anode, Nano Lett. 21 (2021) 7715–7723, doi:10.1021/acs.nanolett.1c02521.

[42] H. Xu, S. Li, C. Zhang, X. Chen, W. Liu, Y. Zheng, Y. Xie, Y. Huang, J. Li, Roll-to-roll prelithiation of Sn foil anode suppresses gassing and enables stable full-cell cycling of lithium ion batteries, Energy Environ. Sci. 12 (2019) 2991–3000, doi:10.1039/c9ee01404g.

[43] B.T. Heligman, A. Manthiram, Elemental foil anodes for lithium-ion batteries, ACS Energy Lett. 6 (2021) 2666–2672, doi:10.1021/acsenergylett.1c01145.

[44] S. Li, Z. Li, L. Huai, M. Ma, K. Luo, J. Chen, D. Wang, Z. Peng, A strongly interactive adatom/substrate interface for dendrite-free and high-rate Li metal anodes, J. Energy Chem. 62 (2021) 179–190, doi:10.1016/j.jechem.2021.03.023.